Analysis of a plastic optical fiber-based displacement sensor

Felipe Jiménez,[1,*] Jon Arrue,[1] Gotzon Aldabaldetreku,[1] Gaizka Durana,[1] Joseba Zubia,[1] Olaf Ziemann,[2] and Christian-Alexander Bunge[3]

[1]University of the Basque Country (UPV/EHU), Alda, Urquijo s/n, E-48013 Bilbao, Spain
[2]POF-AC, University of Applied Sciences, Wassertorstrasse 10, D-90489 Nürnberg, Germany
[3]TU Berlin, Sekr. HFT 4, Einsteinufer 25, D-10587 Berlin, Germany

*Corresponding author: felipe.jimenez@ehu.es

Received 10 April 2007; revised 18 June 2007; accepted 22 June 2007;
posted 25 June 2007 (Doc. ID 81987); published 22 August 2007

An easy-to-manufacture setup for a displacement sensor based on plastic optical fiber (POF) is analyzed, showing computational and experimental results. If the displacement is the consequence of force or pressure applied to the device, this can be used as a force or pressure transducer. Its principle of operation consists of bending a POF section around a flexible cylinder and measuring light attenuation when the whole set is subjected to side pressure. Attenuations are obtained computationally as a function of side deformation for different design parameters. Experimental results with an actually built prototype are also provided. © 2007 Optical Society of America

OCIS codes: 060.2370, 250.5460, 080.2720, 000.4430.

1. Introduction

Plastic optical fibers (POFs) have been used for a whole range of different sensing applications [1,2], mainly due to their robustness, large core diameters, and high numerical apertures, which facilitate handling and light coupling. Some POFs have been employed to sense refractive index [3] or liquid level [4,5], often by making use of light power loss through refraction, or to measure displacement, e.g., by means of diffraction-grating ended POFs [6] or microbends in fibers [7]. In this paper we study an easy-to-manufacture setup for a displacement sensor based on power loss in bends that also serves as a force or pressure sensor, if the displacement is not the magnitude of interest, but a force or pressure applied to the device. A calibration of the device for its use as a weight sensor was carried out by relating different attenuation increases with the corresponding values of the weight applied. The correlation between force and deformation was about 15 N/per mm. However, there are some general differences in the operation of this sensor compared with conventional ones based on bends. First, it employs a particularly high number of turns (20 in the prototype described below) in comparison with other bend sensors based on total internal light reflection (e.g., light was made to turn only 180° in [3] and [4]). This technique improves the performance of a single turn without introducing an excessive attenuation, since the loss in 20 turns is lower than 20 times the loss in one turn. This is due to the redistribution of light along the bent region, which tends to a new equilibrium in its power distribution. Second, in this sensor the shape of the cylinder around which the fiber is bent is changed to a noncircular one, and this fact can be used to improve the linearity of the response curve of the sensor (as will be shown in this paper).

In our displacement or pressure sensor, side compression causes an increase of attenuation in the fiber, which can be measured and related to a specific displacement. Basically, it consists of an elastic cylinder around which a multimode fiber, such as a POF, is bent several times in the shape of a helix (Fig. 1). When the device is subjected to side pressure, due to the displacement of a flat surface in contact with the helical turns, the fiber and the cylinder are compressed (Fig. 2), so the curvature of the fiber axis changes and its cross sections deform, resulting in increased fiber losses.

0003-6935/07/256256-07$15.00/0

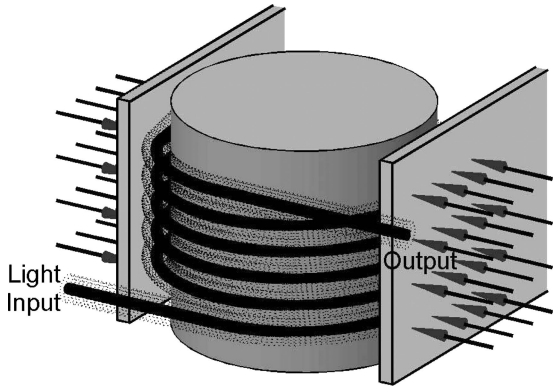

Fig. 1. Fiber bent around a cylinder and pressure applied on the sides, resulting in an increase of light power attenuation.

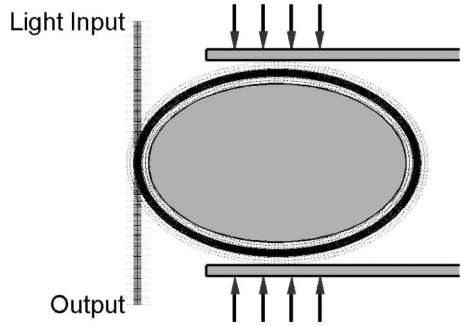

Fig. 3. If the material of the fiber is much stiffer than that of the cylinder, its cross sections remain circular, but its symmetry axis still deforms.

Our study begins with a computational simulation of a prototype actually built at the POF-Application Center (Nürnberg), in which the cylinder is much more flexible than the fiber. The results we obtained helped us to analyze the influence of certain design parameters, such as cylinder radius, numerical apertures of the light source and the fiber, or mechanical properties of the materials employed. The linearity of the curves and their slope (sensitivity) are also discussed. In addition, the methodology and the simplifying hypotheses assumed for the computational simulations are stated, and a model allowing the design of sensors in which the stiffness of the cylinder is comparable with or even much greater than that of the fiber is briefly explained, so as to facilitate work to interested sensor designers.

2. Sensor Setup and Operating Principles

The sensor prototype presented is based on the increase in attenuation taking place when side pressure is applied to a fiber wrapped around a flexible cylinder. When the material of the fiber is much stiffer than that of the internal cylinder, as in the prototype actually built, increases in attenuation are caused mainly by reductions in the curvature radius at some parts of the fiber symmetry axis, assuming that the cross sections of the fiber remain circular (Fig. 3). The parts where the curvature of the fiber axis increases yield higher losses that are only partially compensated by the lower losses taking place where the curvature decreases [8].

In a more general case, both the cylinder and the fiber wrapped around it will undergo deformations when side pressure is applied (Fig. 2). First, the fiber will experience changes of bending radius around the cylinder, leading to additional losses, as explained earlier. Second, and only in the regions where the pressure is applied, the cross sections of the fiber will also undergo deformations that increase power losses above those in the undeformed state.

Deformations of the cross sections of the fiber would cause the predominant effect on attenuation if the material of the cylinder were much stiffer than that of the fiber (Fig. 4). Indeed, the attenuation would tend asymptotically to infinity for a total deformation equal to twice the fiber diameter, because the fiber gets completely flat over a rigid cylinder. In the opposite case (when the material of the fiber is much stiffer than that of the cylinder), we ought to apply a much larger total deformation until the flexible cylinder gets almost completely flat, in which case attenuation would also tend to infinity.

In the prototype, a PFU-CD-501 POF (from Toray Industries, Tokyo, Japan [9]) stripped of its jacket has been used. This POF is a step-index fiber and has

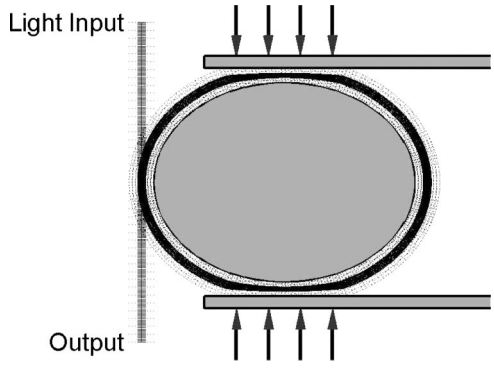

Fig. 2. Both the symmetry axis of the fiber and its cross sections in the proximity of the pressing plane deform to a certain extent.

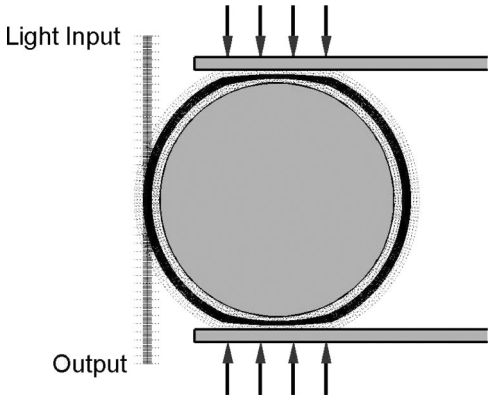

Fig. 4. If the material of the cylinder is much stiffer than that of the fiber, the increase in attenuation is caused mainly by the deformation of the cross sections of the fiber.

a diameter (without a jacket) of 0.5 mm. It has been bent 20 turns tightly, i.e., the pitch of the helix is the minimum possible one. The distance between the symmetry axes of the fiber and the cylinder is 3.5 mm, and the pitch is, very approximately, 0.5 mm. The cylinder is hollow and flexible enough so that the deformations of the cross sections of the fiber can be neglected. Therefore, the symmetry axis of the POF undergoes curvature changes, but its cross sections remain circular. Nevertheless, a computational algorithm to deal with deforming fiber cross sections will also be given.

3. Computational Methodology and Simplifying Hypotheses

A. General Assumptions

The computational simulations were carried out using the implementation of the ray-tracing method described in [10] for step-index POFs of arbitrary three-dimensional geometry. At each reflection or refraction point, a generalized Fresnel transmission coefficient T for curved interfaces, valid for all incident angles and including tunneling rays, has been employed to calculate the fraction of power radiated by the ray into the cladding [11].

Some simplifying hypotheses must be assumed regarding the mechanical behavior of the materials employed. In the first place, all circular cross sections subjected to side pressure will be modeled to deform into elliptical ones. This assumption is probably close enough to the real behavior of both the POF and the internal cylinder. However, in the prototype actually built, the deformations of the cross sections of the POF turn out to be too small to influence attenuations significantly, and therefore the explanations in Subsections 3.B and 3.C will be given in relation to the deformation of the cylinder, leaving the case of significant deformations in the cross sections of the fiber to Subsection 3.D.

B. Cases of Hollow and Solid Flexible Cylinders

First, let us consider the case of a hollow internal cylinder. In this case, the perimeter would be, very closely, invariant under side pressure. Keeping the perimeter constant implies that the area decreases, because the circle is the shape with the greatest area for a given constant perimeter.

Second, let us consider the case of a solid internal cylinder. If it were made of an incompressible material, the area of its cross section would remain nearly constant under side pressure. In mechanical terms, that behavior would correspond to a material with Poisson's ratio equal to 0.5 [12]. However, Poisson's ratio is smaller than 0.5 for most materials, which means that they are compressible to a certain extent. Therefore, it is more realistic to assume that the area of the elliptical cross section of a solid cylinder under side pressure is smaller than the area of a circular, undeformed cross section (as also happens when the perimeter is conserved).

C. Half-Axes of the Deformed Cross Sections

The main conclusion until now is that the real half-axes of a circular cross section deformed into an elliptical one can be assumed to be in the range between the lengths given by the invariance of its perimeter and the invariance of its area, the former case being close to reality when the cylinder is hollow. This leads to the following algorithm that we have used to calculate the deformed half-axes a' and b' of a cylinder of initial (undeformed) radius R.

Let us call d_c the total deformation undergone by the cylinder due to side pressure. Its half-axis $b = R$ will therefore deform into its minor half-axis $b' = R - d_c/2$, since only half of the total deformation goes to each side. If the area were conserved, then $\pi R^2 = \pi a' b'$, so $a' = R^2/b' = R^2/(R - d_c/2)$. We will call this value $a_{area}{}'$. Alternatively, if the perimeter were conserved, $2\pi R = P(a', b')$, where $P(a, b)$ represents the perimeter of an ellipse of half-axes a and b. This cannot be written in a compact form with elementary functions, but it can be computed numerically (or by means of elliptical functions). Thus, we solve numerically for a' the equation $2\pi R = P(a', R - d_c/2)$. Let us call $a_{perim}{}'$ the corresponding solution. According to the information above, the actual minor half-axis a' should lie, very likely, in the range between $a_{perim}{}'$ and $a_{area}{}'$ (and plausibly close to $a_{perim}{}'$ for a hollow, flexible internal rod). We therefore define a parameter k such that

$$a' = a_{area}{}' + k(a_{perim}{}' - a_{area}{}'),$$

i.e., for $k = 0$ the area is conserved, while for $k = 1$ the perimeter is conserved.

D. Deformed State of the Fiber when its Sections Deform Significantly

If the cross sections of the fiber, i.e., not only its symmetry axis, deform significantly under side pressure, further assumptions must be made on the mechanical behavior of the materials employed. When the cross sections of the POF undergo some degree of deformation, not all the displacement sensed by the sensor will be directly translated to the cylinder, but part of it will be absorbed by the fiber. Figure 5 illustrates this situation, where F is the external diameter of the fiber in its undeformed state (0.5 mm in the case of an unjacketed PFU-CD-501 POF), R is the undeformed radius of the cylinder, d is the deforma-

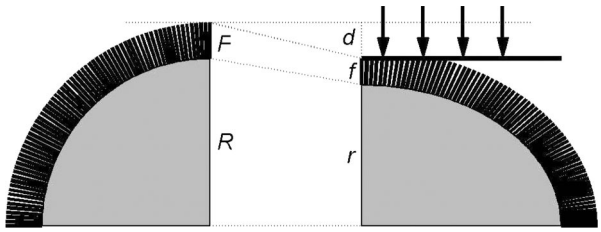

Fig. 5. Assumptions made on the deformations of cylinder and fiber. Parameter q characterizes fiber-to-cylinder maximum unit deformation ratio.

tion undergone by one side of the device (i.e., half of the total deformation), f is the minor axis of the fiber cross section with the greatest deformation, and $r = b'$ is the minor half-axis of the cylinder after deformation. Then, to characterize the cylinder-to-fiber stiffness ratio, we can define a parameter q as the fiber-to-cylinder maximum unit deformation ratio:

$$q = \left(\frac{F}{f} - 1\right) \Big/ \left(\frac{R}{r} - 1\right),$$

which is more convenient to use than the actual fiber-to-cylinder material elasticity ratio.

When the cylinder is rigid and only the POF deforms, $r = R$ and $q = \infty$ (Fig. 4). Conversely, when the material of the cylinder is infinitely flexible in comparison with that of the fiber, $f = F$ and $q = 0$. In a more general case, q will lie somewhere between these two extreme values. Of course, only the cross sections of the fiber sufficiently near the contact area undergo such deformations. Figure 5 shows a sectional view of the cylinder and the fiber in the undeformed (left) and deformed (right) states. The figure was obtained mathematically for a value of q different from 0. As a consequence, those cross sections of the fiber in contact with the mobile plane surface appear deformed, assuming they have become elliptical. In this case, there is a certain area within which the contact between plane and fiber takes place. This area can be calculated as the product of two lengths: the total length of contact shown in Fig. 5 (top), and the length occupied by the N turns of fiber tightly bent along the cylinder axis (which is N times the helical pitch). This area would be 0 for $q = 0$, since the fiber would not deform in such a case (only the cylinder would), so the first of the aforementioned two lengths would be 0. In contrast, such area increases rapidly with q for a fixed total deformation d, the slope being greater for small values of q. For example, using the same geometry as that of the prototype actually built (which will be described below), we have calculated that, for $d = 1$ mm, the area is 0.12 mm^2 when $q = 0.1$; 0.39 mm^2 when $q = 5$; and 0.42 mm^2 when $q = 10$.

Inspecting Fig. 5 helps to derive the equations of the deformed geometry of the fiber. From the equation defining q above, and from $F + R = d + f + r$, we calculate r and f as functions of d, q, R, and F. Once $r = b'$ has been determined, the deformed major half-axis a' of the cylinder is calculated according to its own mechanical properties as explained above: for example, if $k = 0$ (incompressible material), then $a' = R^2/r$.

After calculating half-axes a' and b' of the cross sections of the deformed cylinder, the following algorithm was used, when needed, to calculate the deformed state of the fiber: from any given point of the elliptical boundary of the deformed cylinder, distance F is taken perpendicularly to it. If the end point of that segment lies below the pressing plane (ordinate less than $r + f$), then the corresponding cross section remains in an undeformed, circular state. This happens in a great part of each turn (Fig. 5). However, if the end point of the segment lies above that plane (ordinate greater than $r + f$), then the corresponding minor axis is reduced in the proportion needed so that it ends exactly at the pressing plane, and then the major axis is determined according to the mechanical properties of the fiber (i.e., to parameter k previously discussed, but this time applied to the material of the fiber).

4. Computational and Experimental Results

A. Main Simulation Parameters

An approach generally adopted when using the ray-tracing method [7] consists in modeling only two layers (core and surrounding medium, or core and infinite cladding). Otherwise, the simulation software would have to trace not only ray paths inside the core, but also those traveling through the finite cladding. Including this effect often adds an unmanageable computational cost to the software, since each ray separates into two every time it refracts at the core–cladding interface, leading to an exponentially increasing number of rays to be traced along the fiber.

If the cladding were infinite, radiation losses at tight bends would be significantly higher than in the case of a very thin cladding [13]. Similarly, the simplification of considering that there is no cladding yields lower losses than those obtained with a very thin one, although the difference should not be very large when the cladding is thin [7]. Therefore, in our computational simulations of the prototype built we have treated the unjacketed POF as a 0.5 mm diameter core with a refractive index of 1.492 directly in contact with the surrounding medium (generally air). Nevertheless, the software is also ready to simulate the deformation of the fiber core when it is protected by its jacket (as shown in Figs. 1–4).

Let us now recall the main parameters to be determined at the design stage of the sensor. These are of optical, geometrical, and mechanical nature. The most important optical parameters are the numerical aperture (NA) of the light source (sine of the maximum opening angle of the emitted light in air) and the refractive indices of the core and the external medium. The main geometric parameters are the cylinder radius R, the number of turns of the fiber around the cylinder, and the pitch. The mechanical parameters include the deformation parameter k defined above, and the fiber-to-cylinder maximum unit deformation ratio q (influenced by the choice of cylinder-to-fiber material stiffness ratio). At the design stage, we will assume that the core–cladding interface is not damaged when pressure is applied to it repeatedly. If this occurred in practice, it would cause a great increase in attenuation, so it would be necessary to change the fiber. However, it is very improbable for it to happen, since plastic optical fibers are very resistant. Another issue is the fact that the power emitted by any light source undergoes fluc-

tuations with time. However, there are several alternatives to stabilize the light power. A good solution is to use a reference loop in which another fiber of the same length carries part of the power to a reference photodiode. This alternative cannot only eliminate problems due to changes in emitted power, but also compensate for variations in the receiver sensitivity, spectral drift, and temperature effects on the fiber.

B. Influence of the Numerical Apertures of the Fiber and of the Light Source

We will start by commenting on the prototype actually built. The bend radius of the fiber symmetry axis is very slightly greater than its distance to the axis of the cylinder, i.e., 3.5 mm. Such a small bend radius would produce a strong attenuation in a jacketed POF even in an undeformed sensor, because the jacket is not transparent and its refractive index is similar to that of the core and the cladding. However, the absence of the jacket and the very low refractive index of the outer medium (air, with $n_2 = 1$) make the losses fairly low in the undeformed state of the sensor (a refractive index close to 1 implies a very high numerical aperture of the fiber, which leads to low bending losses). As a matter of fact, bending losses also depend on the filling of the numerical aperture of the fiber achieved with the light source employed, although experimental data obtained with the prototype (Fig. 6) show that attenuation remains very low in the absence of deformation for a very large range of numerical apertures (from 0.09 to 0.65 in the figure). In addition, the rate of increase in attenuation in relation with total deformation (slope of the curves in Fig. 6) rapidly increases with total deformation in all cases. The attenuation was measured in the complete cycle of applying pressure and then releasing it, since there is a small hysteresis cycle. We can see (Fig. 6) that the curves for increasing and decreasing deformations do not coincide exactly.

If the outer medium had a significantly higher refractive index (like water, with $n_2 = 1.33$), the numerical aperture of the fiber would be much smaller, and losses in the fiber would be much higher. For instance, if the surrounding medium were water instead of air, computational calculations for the undeformed state predict a power loss of 0.7 dB instead of 0.07 dB, for a NA of 0.16 and a uniform angular light distribution at the input end (we launch 50,000 rays in the simulations, which is a number in the range between an upper bound delimited by the total number of modes that can propagate within the fiber, and a lower bound to ensure sufficiently smooth and accurate results [7]). This higher attenuation is due to the fact that that light rays refract out of the fiber much more easily if the outer medium is water instead of air. In Fig. 7 we plotted the additional attenuation as a function of the total deformation of the device (relative displacement of the pressing planes) for two different mediums surrounding the fiber, and also for two values of the NA of the light source.

Figure 7 shows two experimental curves and several computational ones. Computational curves obtained with $k = 1$ are probably the most appropriate ones for the prototype actually built, in which the cylinder is hollow and, therefore, the deformation parameter k is expected to be close to 1 (parameter q is expected to be very close to 0, which is the value used in all simulations). The experimental results corresponding to two light sources with a NA of 0.46 and a NA of 0.16 have been plotted. For the sake of com-

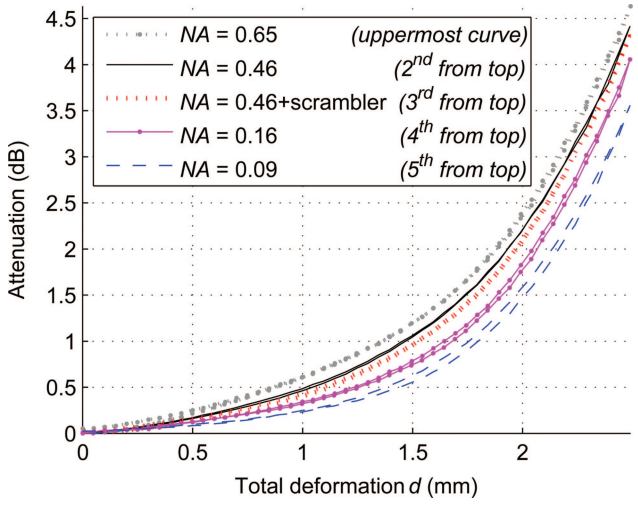

Fig. 6. (Color online) Increase in attenuation in relation with total deformation for different light launching conditions: using a laser followed by different lenses to achieve numerical apertures of 0.65, 0.16, and 0.09, respectively, and using a LED whose numerical aperture is 0.46, with and without a mode scrambler placed after it.

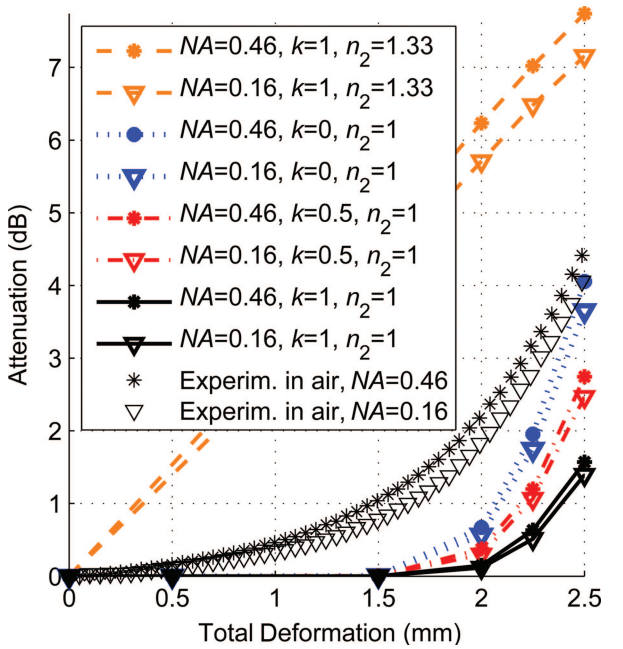

Fig. 7. (Color online) Influence on attenuation of light source NA, deformation parameter k, and refractive index n_2 of the outer medium. When the sensor is in air, $n_2 = 1$; when it is in water, $n_2 = 1.33$.

parison, in all the computational simulations we also considered the same values of the NA of the light source, the unjacketed fiber being surrounded by air or by water. As expected, the higher the NA value, the higher the losses. However, we will see in Subsection 4.D that this effect strongly depends on the radius R of the cylinder.

C. Discussion of the Mechanical Properties of the Internal Cylinder and the Slope of the Curves

Several materials can be employed to make the internal cylinder. In the prototype, it was hollow and made of a very thin layer of steel. Since we do not know the exact value of k to use for the simulations, we plotted results corresponding to three of them (0, 0.5, and 1) for the sake of comparison. As expected, the simulations yield lower values of attenuation than the experimental ones, due to the effect of not including the thin cladding surrounding the core, as commented before. Indeed, although some rays could be trapped in the cladding and come back into the fiber after some reflections, experimental results corroborate that the cladding increases power loss, especially with thicker claddings [13], maybe due to the roughness of the interface. However, we can notice that the slope of the pair of curves for $k = 1$ (expected to be close to the real value) is the most similar one to that of the experimental curve. Additionally, when $k = 0$ the perimeter of the deformed cylinder is larger than with $k = 1$, which implies that the fiber is subjected to smaller bend radii in some parts of each turn around the cylinder. As a result, and for sufficiently large deformations, radiation losses increase much faster for $k = 0$ than for greater values of k, leading to higher attenuations than those expected in the real prototype. We can also notice that the slope would be much greater from the very beginning if the device were immersed in water instead of air (two uppermost curves in Fig. 7). As a matter of fact, $n_2 = 1.33$ for water, so the resulting numerical aperture of the fiber is much smaller, and therefore many rays will undergo refraction even without deformation of the device (a ray loses most of its power when it refracts out of the core). As a result, the slope of the curves is significant also for small deformations, while in air it is practically null until a sufficient degree of deformation starts to make more rays refract out of the fiber (approximately 1.5 mm).

D. Influence of the Radius of the Cylinder

A greater cylinder radius R (e.g., 5 mm) would reduce losses for small deformations even inside water, as shown in Fig. 8, because refraction occurs more easily with smaller bend radii. In the same figure, we can also notice that the increase in attenuation when the numerical aperture of the light source is greater (0.46 instead of 0.16) is more significant when $R = 5$ mm than when $R = 3.25$ mm, since a great number of rays refract with both light sources if $R = 3.25$ mm.

In the case of the prototype working in air, the sensitivity of the sensor is much lower for small total deformations than for large ones. In order to linearize

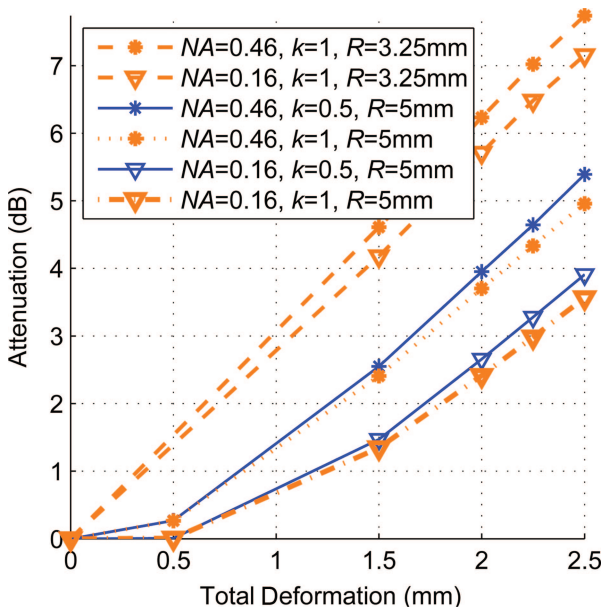

Fig. 8. (Color online) Influence of cylinder radius R on the sensitivity of the device (given by the slope of the lines) when immersed in water.

the whole response curve of the sensor, one possibility is to decrease R. If, for any reason (such as wanting to use an already built sensor) reducing R is not an option, another possibility is to predeform the cylinder conveniently, so as to increase light refraction at very small displacements.

5. Conclusions

An easy-to-manufacture kind of POF-based displacement or pressure sensor has been presented. The influence of some typical optical, geometric, and mechanical design parameters on its sensitivity has been discussed with the aid of computational simulations. The practical viability of the concept has been demonstrated by showing the experimental results of an actually built prototype. It has been shown that its sensitivity is lower for smaller total deformations, and that an increase in radiation losses (e.g., by immersing the device in water, by predeforming the cylinder or by decreasing its radius) tends to increase the small slope exhibited at the beginning of the curves of attenuation as a function of deformation.

This work was supported by the institutions Ministerio de Educación y Ciencia, Universidad del País Vasco/Euskal Herriko Unibertsitatea, and Gobierno Vasco, under projects TEC2006-13273-C03-01, GIU05/03, and HEGATEK-05, respectively.

References

1. T. G. Giallorenzi, J. A. Bucaro, A. Dandridge, G. H. Sigel, Jr., J. H. Cole, S. C. Rashleigh, and R. G. Priest, "Optical fiber sensor technology," IEEE J. Quantum Electron. **QE 18,** 626–665 (1982).
2. D. Kalymnios, P. Scully, J. Zubia, and H. Poisel, "POF sensors overview," in *Proceedings of the Thirteenth International Con-*

ference on Plastic Optical Fibres and Applications—POF'04 (Nürnberg, 2004), pp. 237–244.
3. G. Garitaonaindia, J. Zubia, U. Irusta, J. Arrue, and J. Miskowicz, "Passive device based on plastic optical fiber to determine the index of refraction of liquids," in *Proceedings of the Seventh International Conference on Plastic Optical Fibres and Applications—POF'98* (Berlin, 1998), pp. 178–184.
4. P. Raatikainen, I. Kassamakov, R. Kakanakov, and M. Luukkala, "Fiber-optic liquid-level sensor," Sens. Actuators A **58,** 93–97 (1997).
5. M. Lomer, J. Arrue, C. Jauregui, P. Aiestaran, J. Zubia, and J. M. López Higuera, "Lateral polishing of bends in plastic optical fibres applied to a multipoint liquid-level measurement sensor," Sens. Actuators A **137,** 68–73 (2007).
6. M. Lomer, J. Zubia, J. Arrue, and J. M. López Higuera, "Principle of functioning of a self-compensating fibre-optical displacement sensor based on diffraction-grating ended POF," Meas. Sci. Technol. **15,** 1–5 (2004).
7. J. Arrue, G. Aldabaldetreku, G. Durana, J. Zubia, and F. Jiménez, "Computational research on the behaviour of bent plastic optical fibres in communications links and sensing applications," in *Research Developments in Optics,* 5th issue (Research Signpost, 2005).
8. J. Arrue and J. Zubia, "Analysis of the decrease in attenuation achieved by properly bending plastic optical fibers," IEE Proc. Optoelectron. **143,** 135–138 (1996).
9. Toray Co. Ltd., "Laser components," www.lasercomponents.de/uk/fileadmin/user_upload/home/Datasheets/toray/pofaser.pdf.
10. F. Jiménez, J. Arrue, G. Aldabaldetreku, and J. Zubia, "Numerical Simulation of Light Propagation in Plastic Optical Fibres of Arbitrary 3D Geometry," WSEAS Trans. Mathematics **3, 4,** 824–829 (Corfu, 2004).
11. A. W. Snyder and J. D. Love, "Reflection at a curved dielectric interface—Electromagnetic Tunnelling," IEEE Trans. Microwave Theory Tech. **MTT-23,** 134–141 (1975).
12. E. J. Hearn, *Mechanics of Materials: An Introduction to the Mechanics of Elastic and Plastic Deformation of Solids and Structural Materials,* 3rd ed. (Butterworth-Heinemann, 2001).
13. G. Durana, J. Zubia, J. Arrue, G. Aldabaldetreku, and J. Mateo, "Dependence of bending losses on cladding thickness in plastic optical fibers," Appl. Opt. **42,** 997–1002 (2003).